Temperature Increase on Folded Solar Sail Membranes

Patric Seefeldt[a,*], Bernd Dachwald[b]

[a] *Institute of Space Systems, German Aerospace Center (DLR), 28359 Bremen, Germany*
[b] *Faculty of Aerospace Engineering, FH Aachen University of Applied Sciences, 52064 Aachen, Germany*

Abstract

All currently considered solar sail designs require the deployment of a thin reflective membrane. This membrane is stowed using some folding technique and sometimes coiled onto a spool. The temperature of the deployed sail membrane is a critical aspect for solar sail design. Depending on the geometry of the imprinted folding lines, sunlight may be reflected inside folding lines which would locally increase the temperature of the membrane. The analysis presented here aims for a quantification of that temperature increase. Microscope images of a 7.5 µm thick polyimide membrane reveal the geometry of folding lines for different tensioning states. In addition, the opening of folding lines are analysed with a finite-element beam model. After the determination of the geometry as a function of the tensioning state, it is analysed how many reflections may appear in a folding line depending on its opening angle for a sail that is oriented perpendicular to the Sun. Two cases are investigated, deep space and low-Earth orbit. It is shown that, even for small tensioning states, the membrane geometry does not allow more than only two reflections. Depending on the material, this can cause a slight temperature increase that also depends on the investigated case (deep space or low-Earth orbit).

Keywords: solar sail, hot spots, membrane folding, folding line

Nomenclature

a	Constant for folding line geometry [mm]
A	Earth albedo factor
b	Constant for folding line geometry
F	View factor
E_E	Emitted Earth infrared radiation flux [W/m^2]
q_S	Heat transfer from solar radiation [W/m^2]
q_A	Heat transfer from Earth albedo radiation [W/m^2]
q_{IR}	Heat transfer from Earth infrared radiation [W/m^2]
R	Earth top-of-the-atmosphere radius, 6408 km
r	Solar sail orbit radius [km]
S	Solar constant, 1368 W/m^2
x	Position along centerline of sample [mm]
α	Solar absorptance
ε	Thermal emittance
ψ	Opening angle of folding line [°]
σ	Stefan-Boltzmann constant, 5.67×10^{-8} W/(m^{2}K^4)

1. Introduction

Most solar sail designs (see overview by Gong and Macdonald (2019)) apply folding techniques for stowing the sail membrane for launch. Folding leads to local plastic deformations of the sail membrane, referred to as folding lines (see Fig. 1).

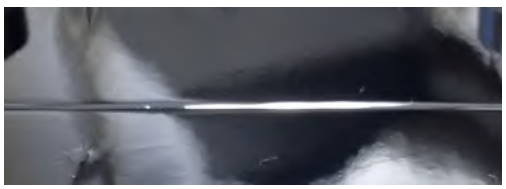

Figure 1: Sail membrane with folding line.

Folding lines in a solar sail membrane may become critical because 1) the coating of the membrane may get

*Patric Seefeldt, patric.seefeldt@dlr.de

damaged at those locations and 2) the geometry of folding lines may lead to multiple reflections of the incident radiation, which could increase the local temperature beyond the membrane's temperature limit. The analysis presented here is a continuation of the work presented by Seefeldt (2018), which focused on the general development and qualification of membranes for space applications.

In Section 2 of this paper, the folding line geometry is determined by microscope measurements. These measurements are then compared to a numerical analysis, in which the folding lines are modelled with finite element methods (FEM), using beams in a non-linear implicit analysis. The path of light rays through the folding line and the impact on the thermal behavior is evaluated in Section 3. This is followed by a discussion of the results in Section 4 and conclusions in Section 5.

2. Measurement of folding line geometry

For our analysis of folding lines, we have prepared samples of UPILEX®-S (7.5 µm thick, 30 mm wide, and 200 mm long, coated with 100 nm of aluminum on both sides) with a folding line in the middle, as shown in Fig. 2(a). As shown in Fig. 2(b), for reproducibility, the folding line was impressed for five minutes with a standard weight of 500 g and a bottom diameter of 38 mm, yielding a defined pressure of about 4323 $\mathrm{N/m^2}$. Afterwards, a thin metal sheet was attached with a transfer adhesive to the sample edges with two threads that allow a uniform tensioning of the sample.

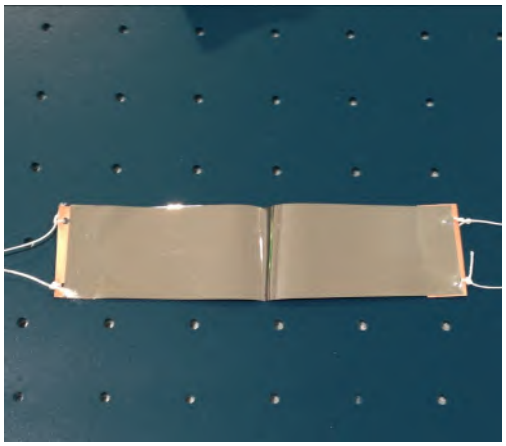

(a) Sample with folding line.

(b) Defined folding of the sample.

Figure 2: Sample for folding line investigation.

2.1. Untensioned folding line

The geometry of an untensioned folding line was measured with a Keyence VR-3200 optical microscope. The microscope generates an ASCII file with Cartesian surface coordinates with a varying resolution of approximately 0.1 mm. Figure 3(a) shows a three-dimensional plot of the surface coordinate points. These surface coordinates were then further processed in order to analyze the geometric profile of the folding line along the centerline of the sample, as shown in Fig. 3(b) (black curve).

It is important to understand that the deformation of the material in the folding line is partially plastic and partially elastic. Therefore, even without a tensioning force, the folding line opens to a certain extend. For an FEM analysis, it is important to derive the load-free geometry of the folding line. Even though the sample was not tensioned, the measurement was carried out under gravity, which slightly increases the opening of the folding line and causes the material to lay flat on the measurement table at some distance from the folding line. But still we considered it to be a good approximation for the derivation of the load-free geometry of the folding line. Without gravity, the folding line would open up according to the stored elastic energy until only the plastic deformation remains and it would keep this geometry also farther away from the folding line (instead of bending over due to gravity). This geometry is shown as the green curve in Fig. 3(b) and it was used as input for the FEM analysis. The used FEM geometry is shown in more detail in Fig. 3(c). With 0.1 mm, the size of the inner radius of the folding line is already in the order of the resolution of the microscope and it already required some estimation and comparison with the electron microscope images of tensioned samples in order to derive the geometry.

For the folding line analysis, the following fit func-

tion was used

$$f(x) = a\,(1 - e^{-bx^2})\,. \tag{1}$$

This function can be used to approximate the opening angle ψ of the folding line at the point x^*, where f has the highest slope:

$$\frac{d^2 f}{dx^2} = 0 \Rightarrow x^* = \pm\frac{1}{\sqrt{2b}}. \tag{2}$$

The opening angle is given by

$$\psi = 2\left[\pi - \tan^{-1}\left(\left.\frac{df}{dx}\right|_{x=x^*}\right)\right] = \\ = \pi - 2\tan^{-1}\left(a\sqrt{\frac{2b}{e}}\right)\,. \tag{3}$$

For the untensioned sample, the function

$$f_{0g}(x) = 4.55\,\mathrm{mm}\left[1 - \exp\left(-0.16\,\frac{1}{\mathrm{mm}^2}\cdot x^2\right)\right] \tag{4}$$

describes the geometry with a standard deviation of 0.3. According to Eq. (3), the opening angle is $\psi = 65.23°$. The red curve in Fig. 3(b) represents this fit function.

2.2. *Tensioned folding line*

In order to analyze tensioned folding lines and the coating inside with greater resolution, a scanning electron microscope from the IWT (Stiftung und Institut für Werkstofftechnik) in Bremen was used. A specifically designed sample holder was employed to measure the topography of folding lines tensioned with different forces. The sample holder and the pre-tensioning principle is shown in Fig. 4. Weights mounted on both sides of the sample apply the load. Two samples were evaluated, one pre-tensioned with 1 g and one pre-tensioned with 125 g on each side. The weight of the sample's overlap with a metal sheet adds another 0.44 g on each side. This results in a tension force of 0.014 N or 6.2×10^4 Pa for the first sample and 1.23 N or 5.47×10^6 Pa for the second sample. After the load is applied, the pre-tensioned sample is fixed by tightening the brackets on top of the sample holder. The weights are disassembled and the overlap of the sample is fixed with Kapton tape on the side of the sample holder. The prepared sample as shown in Fig. 5(a) is then mounted into the microscope's vacuum chamber (see Fig. 5(b)) and the measurement is started.

Figure 5(c) shows a three-dimensional electron microscope image of the bottom of the folding line of the sample that was tensioned with 6.2×10^4 Pa. Inside the

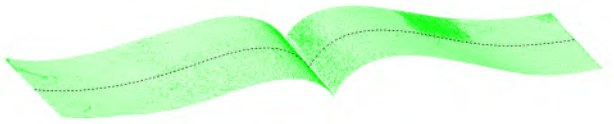

(a) Visualized coordinate points of measurement with Keyence VR-3200 optical microscope. The black dashed line is the profile along the centerline which was used for further geometric analysis.

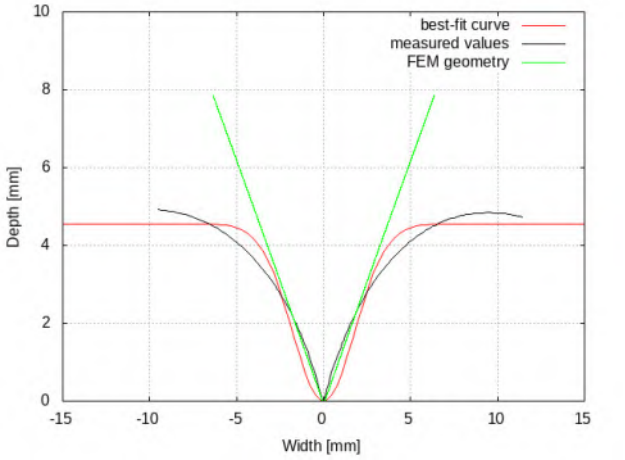

(b) Processed microscope measurements of the folding-line profile along the centerline of the sample, curve of the fit-function according to Eq. (1), and derived FEM initial geometry.

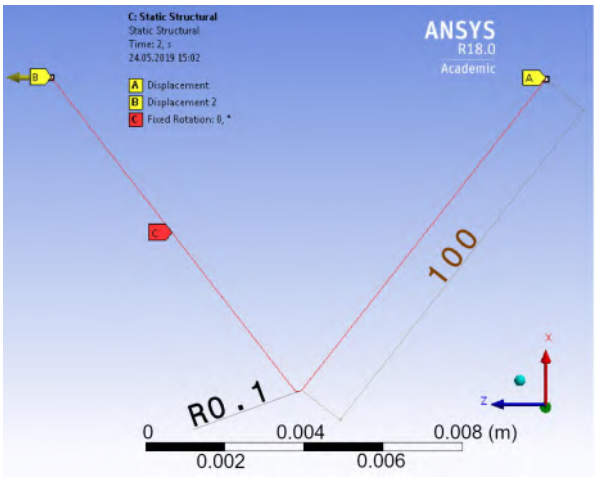

(c) Untensioned folding-line geometry and boundary conditions for FEM analysis.

Figure 3: Folding line according to measurements with Keyence VR-3200 optical microscope.

folding line, some creased lines due to the folding and the general surface roughness are visible. The measured geometry along the centerline of both samples is shown in Fig. 6. For the sample loaded with the 1 g weights,

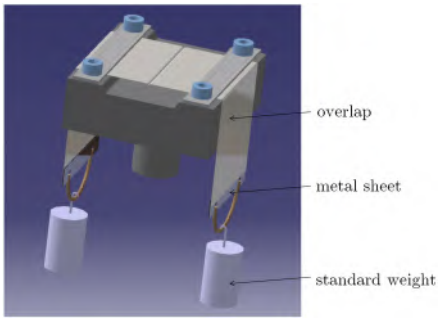

Figure 4: Sample holder for the fixation of samples with pre-tensioned folding lines.

the function

$$f_{1\mathrm{g}}(x) = 0.6\,\mathrm{mm}\left[1 - \exp\left(-2.48\,\frac{1}{\mathrm{mm}^2}\cdot x^2\right)\right] \quad (5)$$

describes the geometry with a standard deviation of 0.044. The opening angle is $\psi_{1\mathrm{g}} = 102°$. For the sample loaded with the 125 g weights, the function

$$f_{125\mathrm{g}}(x) = 0.06\,\mathrm{mm}\left[1 - \exp\left(-14.28\,\frac{1}{\mathrm{mm}^2}\cdot x^2\right)\right] \quad (6)$$

describes the geometry with a standard deviation of 0.015. The opening angle is $\psi_{125\mathrm{g}} = 158°$.

3. Hot spots in folding lines

Inside a folding line, multiple reflections of incident light may cause a local increase in temperature. These hot spots depend on the light incidence angle and the folding-line geometry, which in turn depends on the tension of the membrane. Figure 7 illustrates that the number of reflections depends on the opening angle ψ of the folding line. For $\psi < 90°$, multiple reflections inside the folding line occur. For $90° \leq \psi \leq 120°$, however, only two reflections occur, and for $\psi > 120°$, only one reflections occurs so that no hot spot can form.

3.1. Hot-case scenarios for sail membrane without folding lines

We first investigate the maximal temperature of a flat sail membrane without folding lines for 1 au solar distance in deep space and for low-Earth orbit (LEO). For the hot-case in deep space, the sail membrane is facing the Sun and is only illuminated by direct solar radiation. Therefore, the total heat transfer to the sail membrane per unit area results from the absorbed direct solar radiation flux, $q_S = \alpha S$. In equilibrium, the (infrared) radiation flux emitted by the sail membrane is

(a) Sample tensioned with a weight of 125 g fixated with the brackets on the sample holder.

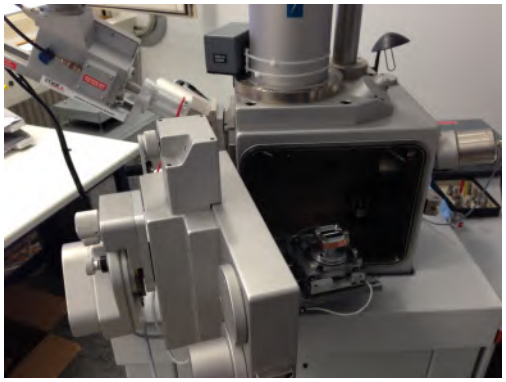

(b) Scanning electron microscope of the IWT Bremen with sample holder and sample mounted inside the microscope's vacuum chamber.

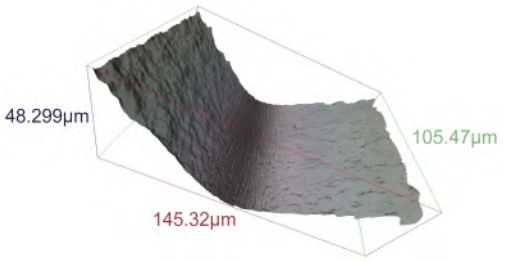

(c) Microscopic three-dimensional image of folding line

Figure 5: Microscopic investigation of folded sample.

$\varepsilon\sigma T_{\max}^4 2A_s$ and the hot-case temperature is then calculated from $q_S = 2\varepsilon\sigma T_{\max}^4$ as

$$T_{\max} = \left(\frac{q_S}{2\varepsilon\sigma}\right)^{\frac{1}{4}} = \left(\frac{\alpha S}{2\varepsilon\sigma}\right)^{\frac{1}{4}}. \quad (7)$$

For the hot case in LEO, the solar sail is at the subsolar point and the sail membrane is facing the Sun (see Fig. 8). In this case, the sail membrane receives solar radiation (direct and albedo) and Earth infrared radiation.

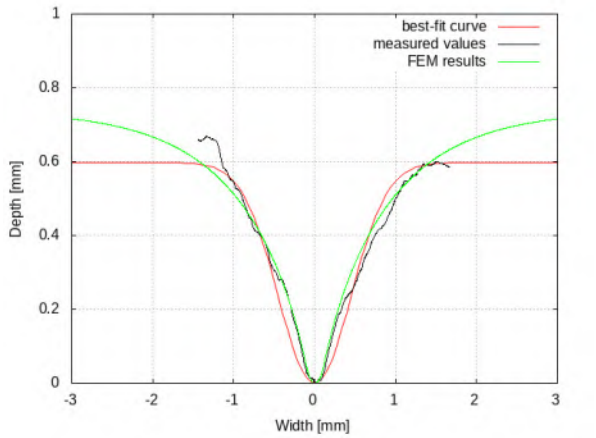

(a) Best-fit curve (red) according to Eq. (5) and FEM results (green) for the folding line (black) which was tensioned with 0.014 N (6.2×10^4 Pa).

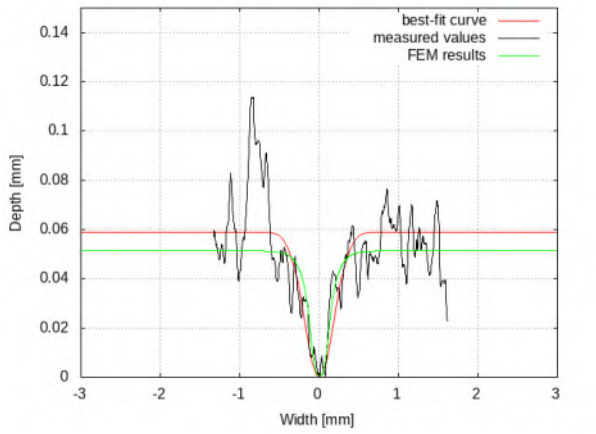

(b) Best-fit curve (red) according to Eq. (6) and FEM results (green) for the folding line (black) which was tensioned with 1.23 N (5.47×10^6 Pa).

Figure 6: Measured geometry of the folding line in the middle of the sample, curves of fit function according to Eq. (1) and FEM results.

The view factor F for this geometry is

$$F = \left(\frac{R}{r}\right)^2 , \tag{8}$$

where r is the solar sail's orbit radius, here 6678 km, and $R = 6408$ km is Earth's top-of-the-atmosphere radius (see Gilmore (2002)). The total heat transfer to the sail membrane, as illustrated in Figure 9, has three contributions: 1) the absorbed direct solar radiation flux, $q_S = \alpha S$; 2) the absorbed Earth albedo radiation flux, $q_A = \alpha F A S$, where A is the Earth albedo factor; and 3) the absorbed Earth infrared radiation flux, $q_{IR} = \varepsilon F E_E$, where E_E is the emitted Earth infrared radiation flux. Following the recommendations given by Gilmore (2002), the chosen values for the Earth albedo factor and the emitted Earth infrared radiation flux are $A = 0.38$ and $E_E = 315\,\mathrm{W/m^2}$, respectively. The absorbed Earth infrared radiation flux then becomes $q_{IR} = \varepsilon F E_E$. The hot-case temperature is then calculated from $q_S + q_A + q_{IR} = 2\varepsilon\sigma T_{\max}^4$ as

$$\begin{aligned} T_{\max} &= \left(\frac{q_S + q_A + q_{IR}}{2\varepsilon\sigma}\right)^{\frac{1}{4}} \\ &= \left(\frac{\alpha(1 + FA)S + \varepsilon F E_E}{2\varepsilon\sigma}\right)^{\frac{1}{4}} . \end{aligned} \tag{9}$$

Figure 10 shows the hot-case temperatures for both cases for different α/ε ratios. Seefeldt (2018) measured an α/ε ratio of 0.731 for a membrane coated with aluminum, silicon dioxide and titanium dioxide, and an α/ε ratio of 2.54 for a membrane with pure aluminum coating. Figure 11 shows the temperature difference between both cases for different α/ε ratios

3.2. Hot-case scenarios for sail membrane with folding lines

For the hot-case scenarios described in section 3.1, we now analyze the reflection of radiation within a folding line of a sail membrane that is directed perpendicular to the Sun. In the following, we analyse the case $90° \leq \psi \leq 120°$, where only two reflections occur. This is reasonable, since the results in section 2.2 have shown that even for low tensioning forces, ϕ becomes larger than 90°. The temperature increase inside such a folding line can be estimated under the following simplifying assumptions:

1. Reflections inside the folding line are purely specular. No diffuse reflection takes place.
2. The diffusely emitted infrared radiation of the sail membrane inside the folding line can be neglected, because it does not considerably contribute to the temperature increase.

We first consider the sail membrane at 1 au solar distance in deep space, facing the Sun (i.e. without q_A and q_{IR}). The absorbed solar radiation flux is

$$q_S = \alpha S \cos\left(\frac{\pi}{2} - \frac{\psi}{2}\right) = \alpha S \sin\left(\frac{\psi}{2}\right) . \tag{10}$$

The reflected solar radiation flux is (specular reflection)

$$(1 - \alpha)\, S \sin\left(\frac{\psi}{2}\right) \tag{11}$$

and the part of it that is absorbed by the opposite side of the folding line, at the hot spot, is, as a simple geometrical analysis reveals,

$$q_2 = \alpha\,(1 - \alpha)\, S \sin\left(\frac{\psi}{2}\right) \sin\left(\frac{3\psi}{2}\right) . \tag{12}$$

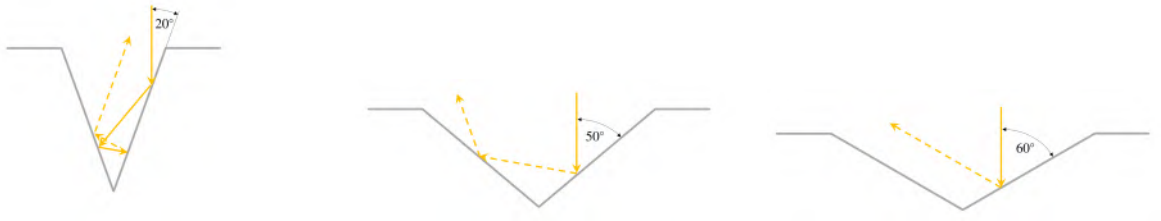

(a) Multiple reflections for small opening angles $\psi < 90°$, here $\psi = 40°$

(b) Two reflections for medium opening angles $90° \le \psi \le 120°$, here $\psi = 100°$

(c) Single reflection (and no hot spot) for large opening angles $\psi > 120°$, here $\psi = 120°$.

Figure 7: Path of the incident solar radiation for different opening angles of the folding line.

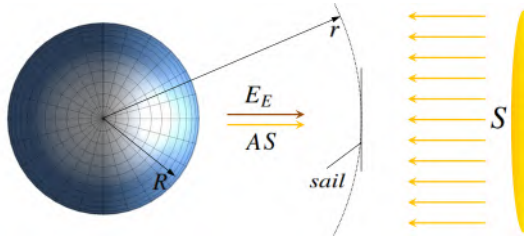

Figure 8: Illustration of the hot case for a sail in a low-Earth orbit at sub-solar point with Earth (top-of-the-atmosphere) radius R, solar sail orbit radius r, solar constant S, Earth albedo factor A and emitted Earth infrared radiation flux E_E.

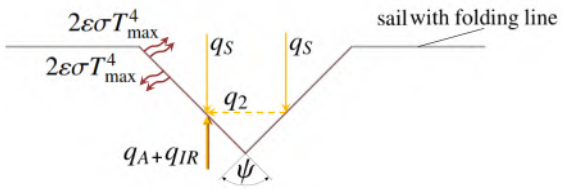

Figure 9: Heat transfer to a sail membrane with a folding line (here, $\psi = 90°$) facing the Sun.Transfer of heat to a point in the folding line is due to solar radiation, q_S, and reflection in the folding line, q_2. In case the sail is in an Earth orbit, additional heat transfer due to Earth albedo, q_A, and Earth infrared radiation, q_{IR}, are present.

The hot-case temperature at the hot spot is then calculated from $q_S + q_2 = 2\varepsilon\sigma T^4_{\max}$ as

$$T_{\max} = \left(\frac{q_S + q_2}{2\varepsilon\sigma}\right)^{\frac{1}{4}} . \tag{13}$$

Figure 12 shows the estimated temperature increase inside a folding line with respect to a flat sail membrane for the deep space case.

For the sail membrane in LEO at the subsolar point, the situation is a bit more complex, because the backside of the folding line is illuminated by Earth albedo and by Earth infrared radiation (see Fig 9). The view factor for

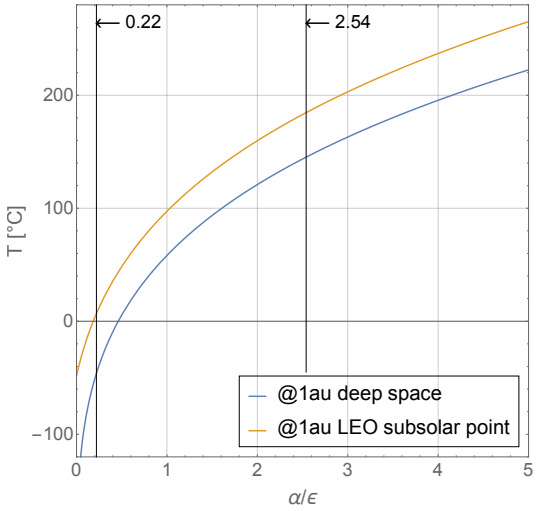

Figure 10: Hot-case sail membrane temperature as a function of α/ε for deep space at 1 au solar distance and for LEO at the subsolar point.

the backside of a folding line is

$$F = \left(\frac{R}{r}\right)^2 \cos\left(\frac{\pi}{2} - \frac{\psi}{2}\right) = \left(\frac{R}{r}\right)^2 \sin\left(\frac{\psi}{2}\right) . \tag{14}$$

Using this view factor, the absorbed radiation flux from Earth albedo is again $q_A = \alpha FAS$ and the absorbed radiation flux from Earth infrared radiation is again $q_{IR} = \varepsilon F E_E$, as for the flat sail membrane. The hot-case temperature at the hot spot is then calculated from $q_S + q_2 + q_A + q_{IR} = 2\varepsilon\sigma T^4_{\max}$ as

$$T_{\max} = \left(\frac{q_S + q_2 + q_A + q_{IR}}{2\varepsilon\sigma}\right)^{\frac{1}{4}} . \tag{15}$$

Figure 13 shows the estimated temperature increase inside a folding line with respect to a flat sail membrane for the deep space case.

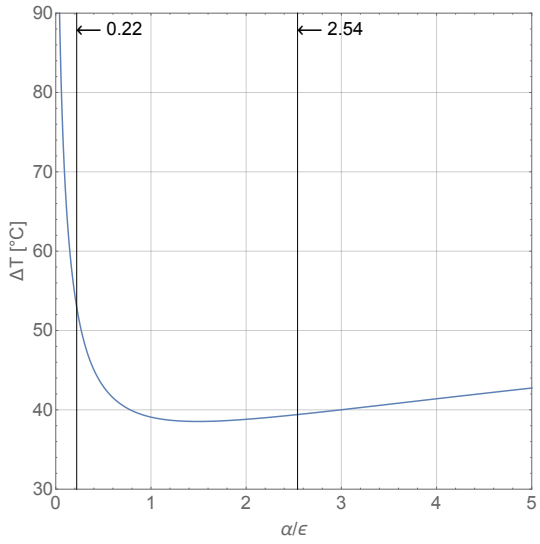

Figure 11: Difference between the hot-case sail membrane temperature as a function of α/ε for LEO at the subsolar point and for deep space at 1 au solar distance.

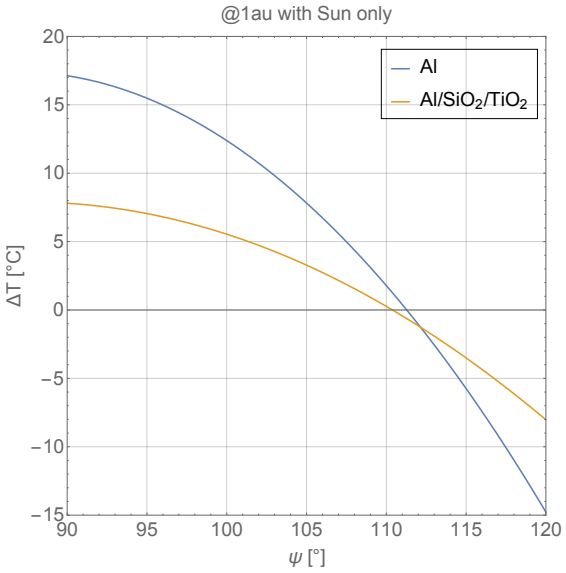

Figure 12: Temperature difference due to two reflections in the folding line for the deep space case (1 au). Positive values indicate a temperature increase.

4. Discussion

The temperature of a solar sail membrane at 1 au depends on whether or not the albedo and infrared radiation from Earth is present as well as on the α/ε ratio of the membrane (see Figs. 10 and 11). As expected, temperatures are higher in proximity to the Earth due to the additional radiation fluxes it provides. For reasonable ratios $0.5 < \alpha/\varepsilon < 5$, the difference is $\approx 40\,^{\circ}\mathrm{C}$.

The temperature increase in folding lines also depends on Earth presence and the α/ε ratio of the membrane (see Figs. 12 and 13). In the cases that we have investigated, the temperature increase at 1 au distance from the Sun can be as much as about 17°C for a membrane with $\alpha/\varepsilon = 2.54$ and about 10.5°C for a membrane with $\alpha/\varepsilon = 0.731$.

The temperature difference decreases with increasing folding line angle ψ, which might be expected, but it can also becomes negative for larger angles. This is due to the smaller light incidence angles in folding lines as compared to the flat membrane. This becomes more clear when considering the whole folding line area. The area projected into the direction of the incoming radiation is smaller than the surface area of the folding line. In total, less radiation power per surface area is entering the folding line as compared to the flat area. Therefore, areas with elevated temperatures due to absorbed reflected radiation (hot spots) are expected to be local.

Close to Earth, although the sail has a higher temperature as compared to the deep space case, the temperature difference is smaller and can even be negative for all opening angles $\psi > 90°$. This may seem a bit counterintuitive. However, due to the folding line, the backside of the sail membrane receives less radiation power per unit area than a flat membrane. This effect gets stronger with increasing folding line angle ψ and for membrane materials with lower α/ε. With a low enough α/ε the temperature in the folding line can always be smaller for all opening angles $\psi > 90°$.

5. Summary and conclusions

We have investigated the folding line in a 7.5 µm thick UPILEX®-S polyimide coated on both sides with Aluminium. The analysis of folding lines requires geometry information on a very small scale down to 10^{-2} mm. An optical and an electron microscope gave accurate measurements of the folding lines geometry. For modelling and simulation, it is important to have information about the folding line in its untensioned state. The deformation when imprinting the folding line is partly elastic. Therefore, the fold is opening to a certain extend without any force and the inner radius of the folding line is less sharp than it may be expected.

Having this geometric information allows a simulation of the folding line in different tensioning states with a simple beam model in a non-linear implicit analysis. This simulation provides a complete picture of the opening process of a folding line.

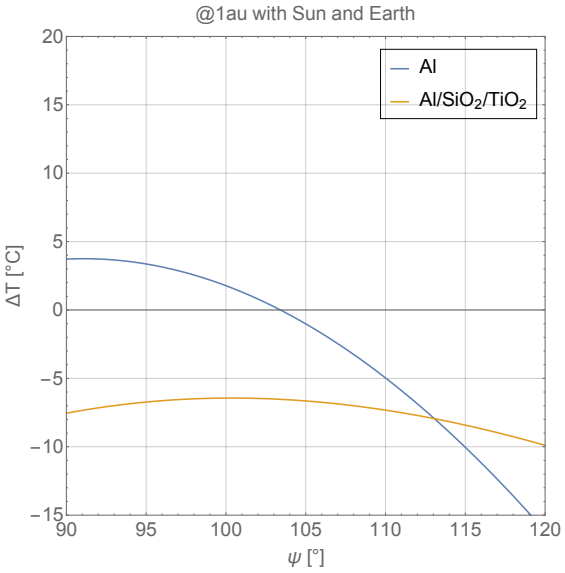

Figure 13: Temperature difference due to two reflections in the folding line for the LEO sub-solar point case. Positive values indicate a temperature increase.

The fit function that was used in this paper represents the geometry of a folding line to a certain extend (e.g. the minimum opening angle) but is not very accurate in modelling the curvature at the very inside of the folding line and in the transition zone to the flat areas. In the future, it could be explored to consider elliptic integrals for this problem, as described in (Timoshenko and Gere, 2009, pp. 76-82). Still, in order to describe the inner curvature of the folding line, an adaptation would be required.

The folding line geometry shows that already slight tensioning is enough to reduce the amount of reflections inside the folding line to two. In order to estimate the temperature increase inside the folding line, a simplified case with two reflections was studied. The local temperature increase due to these reflections compared to the flat sail is estimated to be less than about 17 °C for an aluminized membrane. In this calculation, however, it is not considered that conduction inside the membrane material would lead to a reduction of a local increase in temperature.

Considering that current aluminized membranes are operating at temperatures about 170 °C (worst case in a low-Earth orbit) this increase is low. Furthermore, the currently considered polyimide materials have temperature limits of a few hundred degrees Celsius (depending on the manufacturer), which still leaves enough margin for such an increase.

For missions closer to the Sun, where higher temperatures are expected, it should be considered to establish a requirement defining a minimum tension perpendicular to the folding line that ensures that only two reflections are present.

Acknowledgements

The authors would like to thank the students Christoph Auenmüller, Chris Nordmann and Benedikt Wermann, who supported this work with their theses.

References

Gilmore, D. (Ed.), 2002. Spacecraft Thermal Control Handbook, Volume I: Fundamental Technologies. 2nd ed., The Aerospace Press, El Segundo, CA.

Gong, S., Macdonald, M., 2019. Review on solar sail technology. Astrodynamics 3, 93–125, https://doi.org/10.1007/s42064–019–0038–x.

Seefeldt, P., 2018. Development and Qualification of Deployable Membranes for Space Applications. Ph.D. thesis. Universität Bremen.

Timoshenko, S.P., Gere, J.M., 2009. Theory of elastic stability. 2 ed., Dover Publications, INC, Mineola, New York.